Coherency saturation in periodic structures with randomization

Alexander E. Kaplan and Sergey G. Zykov

Department of Electrical and Computer Engineering, Johns Hopkins University, Baltimore, Maryland 21218

Received January 6, 2004; revised manuscript received September 9, 2004; accepted October 2, 2004

We study the effect of coherency saturation in spatially or temporally periodical structures with randomization, applicable to a very broad class of systems. We derive a simple analytical formula in the case of uncorrelated deviations of periods with Gaussian probability distribution. Using Monte Carlo simulations, we also demonstrate that many other distributions show statistical properties that closely coincide with the Gaussian, although some of them are drastically different from it. We observed that the characteristic number of elements necessary for the saturation of the coherency (the "coherency range") depends only on the normalized standard deviation of the size of the elements and not on their probability distribution function. A greatly simplified heuristic formula found by us also fits all of these results with very reasonable precision. In the specific case of x ray transition radiation of low-to-medium relativistic electron beams in multilayer solid-state nanostructures, we show that a structure of a few hundred layers can generate resonantly enhanced radiation in the hard x ray domain with almost unhampered coherency gain.

OCIS codes: 030.1640, 230.1950, 230.4170, 260.3160.

1. INTRODUCTION

An ancient legend states that when the Syracuse was under naval siege, Archimedes assembled Syracusean soldiers at the beach and instructed them to direct the sunlight reflected from their polished shields into the sails of enemy ships. The sails caught fire, and the siege was defeated. As a predecessor of laser SDI (Strategic Defense Initiative), this legend makes a nice example of the science being good for homeland security, but the focusing efficiency (or the spatial coherency of the reflected light) of such an almost-random optical structure is far from optimal. Many manmade or naturally occurring structures have much better design, but the problem of the coherency of (somewhat) randomized quasi-periodic structures remains essential for their performance as antennas, radiators, mirrors, etc. This problem permeates many areas of physics and technology: antennas and radar arrays in radio, *mw*,[1–3] optical domains (in particular, diffraction gratings[4–6]), and acoustics[7–9]; multilayer interference filters and mirrors, including Bragg reflectors for fiber optics[10] and x ray laser mirrors[11–13]); *mw* undulator and optical free-electron lasers[14–16]; multilayer structures for x ray transition radiation of relativistic electrons[17–20]; Alfven waves[21]; atomic optics[22]; and photonic crystals,[23–25] etc. A temporal analogy of these spatially periodic systems is the generation of a train of short pulses by frequency-equidistant multimodes in a mode-locked laser,[26] whereby the intensity and duration of pulses is determined by the coherence or the spacing of the participating modes. The most recent example of this kind of process is the generation of subfemtosecond pulses based on the equidistant comb of either higher-order harmonics[27,28] or multicascade stimulated Raman scattering.[29–31] A major example of naturally occurring spatially periodic systems is solid-state crystal, whose spatial periodicity is at the core of quantum solid-state theory and classical Bragg reflection; the spatial coherency of many effects in the crystal is determined by its statistical properties.[32–34]

Perhaps the best way to quantify the coherence of the multielement structure is to look at the intensity of the signal from these systems in the far-field area. If the total number of elements is M, and they are ideally equidistant, the ideal coherency gain G of the intensity of the radiation in the maximum of the main lobe (e.g., first maximum in the diffraction grating), compared to that from a single element, is

$$G_{\mathrm{coh}}(M) = M^2. \tag{1}$$

This is the situation common to many wave–oscillation problems, whereby owing to the fully constructive interference for the right conditions (e.g., the angle of radiation for a fixed frequency, or vice versa) in the far-field area, the amplitude E_{ff} of the radiation is the sum of all of the individual amplitudes, i.e., it is proportional to M, and therefore the total intensity is proportional to M^2. In the opposite case of randomly positioned elements, the expected gain is simply

$$G_{\mathrm{rand}}(M) = M, \tag{2}$$

since now only the intensities add up; it is called here the "Archimedes' limit."

In this paper, we study the randomization-induced inhibition of coherency of multielement arrays from a very generic point of view and develop a very simple theory of the phenomenon, which is universally characterized by what we call here coherency saturation, whereby the coherent enhancement $G(M)/M$ reaches its upper limit as the number of elements M increases beyond some characteristic scale of randomization, or "coherency range" N_{coh}.

In Section 3, using the generic statistical model outlined in Section 2, we obtain the exact analytical formula

distribution for the normal (Gaussian) statistical distribution of the spacing between the elements. It is then explored in Section 4 in detail for the case of "exact resonance," including simplified approximations and an even simpler heuristic formula. These analytical results for the normal (Gaussian) distribution are then thoroughly compared in Section 5 with six other realistic models of statistical distribution by use of numerical Monte Carlo simulations for those models. These models include such widely varying distributions as rectangular, smooth-with-hard-edges, and four different smooth distributions. As one can expect these models showed the results to be approaching that of the analytically solvable Gaussian distribution for $N_{\mathrm{coh}} \gg 1$, due to the central limiting theorem of the probability theory; however, amazingly enough, all of them stayed very close to the Gaussian model results down to the coherency range as low as $N_{\mathrm{coh}} \sim 2$. Using the general analytical results of Sections 2 and 3, we also consider in Section 6 the transformation of angular diagrams (which correspond to a nonresonant case) owing to coherency saturation and show that they rapidly degenerate from the familiar $\cos^2(M\pi\theta)/(\pi\theta)^2$ shape into a regular Lorentzian profile with its width determined by N_{coh}^{-1} if $M \gg N_{\mathrm{coh}}$. Finally, we consider, as an example, the tolerance requirements for the thickness of layers in the multilayered solid-state structure for the x-ray transition radiation in Section 7.

2. STATISTICAL MODEL

We assume that the spacings l_n between any adjacent elements randomly deviate (with no correlation between them) from some design optical length l_0, and the standard deviation $\sigma_l < l_0$ is the same for all of them. We will consider here the most important case of the so-called first maximum (or first resonance), whereby the phase difference between the radiation attributed to two adjacent elements is near 2π:

$$\phi_n = 2S\pi l_n/\lambda = 2\pi(1 + \theta + x_n), \tag{3}$$

where λ is the wavelength of radiation, $\theta \ll 1$ is a fixed, nonrandom detuning from the exact resonance, x is a random variable with the symmetric probability distribution $P(x) = P(-x)$, and

$$\langle x_n \rangle = 0, \qquad \langle x_n^2 \rangle = \sigma_0^2 = \sigma_l^2/l_0^2, \tag{4}$$

where σ_0 is a normalized standard deviation and S is a system-specific parameter. (For example, for the diffraction grating one has $S = \sin(\psi)$, where ψ is the angle between the direction of observation and the direction normal to the grating plane. Note that the spacing l can be much larger than λ; e.g., for $S \approx \psi \ll 1$. For S in the case of the transition radiation, see Eq. (37) below. Counting the phase from the very first element (so that $\phi_1 = 0$), we have the amplitude of the signal coming in far-field area from the nth element (relative to the amplitude from a single, e.g., the first element) as

$$f_n = \exp[2\pi i(X_n + n\theta)], \tag{5}$$

with $X_n = \Sigma_{j=1}^{n} x_n$, where $2\pi X_n$ is an accumulated phase at the nth element. The total (relative) amplitude of the radiation, F_M, is then

$$F_M = \sum_{n=1}^{M} f_n, \tag{6}$$

and the respective (relative) intensity, averaged over a statistical ensemble, is what we are looking for, the coherency gain:

$$G_M = \langle |F_M|^2 \rangle = \left\langle \left| \sum_{n=1}^{M} \exp[2\pi i(X_n + \theta n)] \right|^2 \right\rangle, \tag{7}$$

where angular brackets designate the averaging over the ensemble. We can now transform Eq. (7):

$$\begin{aligned} G_M &= \left\langle \sum_{n,k=1}^{M}\sum \exp\{2i\pi[X_n - X_k + (n-k)\theta]\} \right\rangle \\ &= \frac{1}{2}\left\langle \sum_{n,k=1}^{M}\sum (\exp\{2i\pi[X_n - X_k + (n-k)\theta]\} \right. \\ &\quad \left. + \text{c.c.}) \right\rangle \\ &= \sum_{n,k=1}^{M}\sum \{\langle \cos[2\pi(X_n - X_k)]\rangle \cos[2\pi(n-k)\theta] \\ &\quad - \langle \sin[2\pi(X_n - X_k)]\rangle \sin[2\pi(n-k)\theta]\}. \end{aligned} \tag{8}$$

Since the probability distribution is symmetrical, we have $\langle \sin[2\pi(X_n - X_k)]\rangle = 0$ and

$$G_M = \sum_{n,k=1}^{M}\sum \cos[2\pi(n-k)\theta]\langle \cos[2\pi(X_n - X_k)]\rangle, \tag{9}$$

where the term $\langle \cos[2\pi|X_n - X_k|]\rangle$ can be readily evaluated. The amount $X_n - X_k = \Sigma_{j=k}^{n} x_j \equiv Y_{nk}$ is the sum of many uncorrelated random variables x_j, each one having the same probability distribution.

3. NORMAL (GAUSSIAN) DISTRIBUTION OF INTERVALS

Let us consider first the case of a normal (Gaussian) distribution of spacings between any adjacent elements, whereby the probability density function of these spacings is as follows:

$$P(x) = (\sigma_0\sqrt{2\pi})^{-1} \exp(-x^2/2\sigma_0^2),$$

and, as stressed in Section 2, their deviations are uncorrelated with each other. Owing to Eq. (4), $\langle Y_{nk}\rangle = 0$, and the probability distribution for $y = Y_{nk}$ is also Gaussian:

$$P_{nk}(y) = \frac{1}{\sigma_{nk}\sqrt{2\pi}} \exp\left(-\frac{y^2}{2\sigma_{nk}^2}\right), \tag{10a}$$

where

$$\sigma_{nk}^2 \equiv \langle Y_{nk}^2\rangle - \langle Y_{nk}\rangle^2 = |n-k|\,\sigma_0^2, \tag{10b}$$

so that

$$\langle \cos(2\pi Y_{nk}) \rangle = \int_{-\infty}^{\infty} \cos(2\pi y) P_{nk}(y) dy$$

$$= \exp(-2\pi^2 \sigma_0^2 |n - k|). \quad (11)$$

Note that owing to the central limit theorem, for sufficiently large $|n - k|$ (for most realistic models, a very low $|n - k|$ does the job), the amount Y_{nk} is also expected to be distributed normally regardless of the model of the probability distribution (for more details, see below), if again the deviations of the adjacent spacings are uncorrelated. The latter assumption is to a great extent a worst-case scenario, albeit realized in many situations of interest. In the case of a correlation between neighboring spacing deviations, the theory should be further advanced by considering the correlation function between those deviations via the joint probability density function, which is beyond the scope of this paper.

4. COHERENCY SATURATION AT THE EXACT RESONANCE ($\theta = 0$)

Defining the randomization parameter r and the inverse to it, the coherency range N_{coh} as

$$r = (\pi \sigma_0)^2, \qquad N_{\text{coh}} = r^{-1}, \quad (12)$$

substituting the result [Eq. (11)] into Eq. (9), and looking first into the case of exact resonance $\theta = 0$ we arrive at the relationship

$$G_M(\theta = 0) = \sum_{n,k=1}^{M} \exp(-2r|n - k|)$$

$$= \frac{(M/2)\sinh(2r) - \exp(-rM)\sinh(rM)}{\sinh^2(r)}. \quad (13)$$

A quick check verifies the expected properties of G_M. Indeed, $G_M = 0$ at $M = 0$, $G_M = 1$ at $M = 1$, and in the full randomization limit, $r \to \infty$, we have $G_M \to M$, as expected; also, in the full coherency limit, $r \to 0$, we have $G_M \to M^2$. The behavior of $\mathcal{E} \equiv G_M/M$ as function of M for various standard deviations σ_0 is depicted in Fig. 1.

Typically, there is at least some coherence, i.e., $r \ll 1$, or $N_{\text{coh}} \gg 1$, and the exact solution [Eq. (13)] can then be reduced to a simpler formula:

$$G_M(\theta = 0) = N_{\text{coh}}^2[\mu - \exp(-\mu)\sinh(\mu)], \quad (14a)$$

with

$$\mu = Mr = M/N_{\text{coh}}. \quad (14b)$$

Note also that under the condition $N_{\text{coh}} \gg 1$ one can assume Gaussian statistics for the sum Y_{nk} regardless of the probability distribution for individual spacing x_n (see also below), so Eq. (14) is then true for a large class of probability distributions. The result [Eq. (14)] can also be obtained from Eq. (13) if we replace the summation by the integration. It is worth noting that, contrary to common intuitive expectation, $N_{\text{coh}} \propto \sigma_0^{-1}$, we have $N_{\text{coh}} \propto \sigma_0^{-2}$, which promises a very robust coherency of these periodic structures in most realistic situations. For example, assuming the tolerance of $\sigma_0 \sim 1\%$, which is well within the state-of-the-art technological capabilities in many domains, including x-ray domain, one can put together $M \sim 1000$ elements and still retain ~50% of the ideal gain, $G_{\text{coh}} = 10^6$.

From now on, it would be convenient and instructive to use the notion of the coherency enhancement, $\mathcal{E} = G_M/M$ of the full gain G_M over the fully incoherent, random structure gain M. Thus in the case of full coherence $\mathcal{E} = M$, and in that of fully random system, $\mathcal{E} = 1$. Using Eq. (14), one gets the formulas for small perturbation in the strong-coherence limit

$$\mathcal{E}(M) \approx M(1 - 2\mu/3), \qquad \mu \ll 1, \quad (15)$$

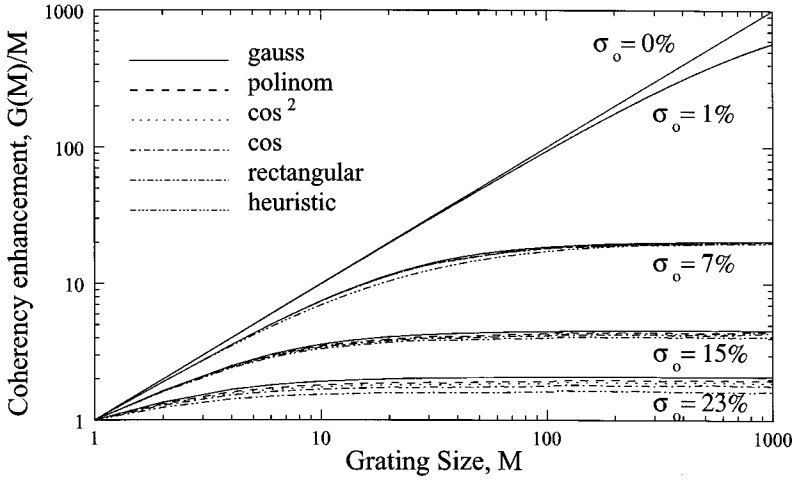

Fig. 1. Coherency enhancement $\mathcal{E} = G_M/M$ versus the number M of elements in the structure for various models of probability distributions, and various standard deviations, σ_0. The upper straight line $\mathcal{E} = M$ is due to the fully coherent structure ($\sigma_0 = 0$), whereas $\mathcal{E} = 1$ is due to the fully randomized ($\sigma_0 = \infty$) structure. The rest of the lines correspond to $\sigma_0 = 1\%$, 7%, 15%, and 23% from top to bottom, respectively. Each group of curves corresponding to each specific σ_0 consists of a solid curve due to the exact analytical result [Eq. (13)] for a Gaussian statistical distribution of the spacings and four others due to the models [Eqs. (20)–(23)] and was obtained by Monte Carlo simulations. The dotted curve in the group that corresponds to $\sigma_0 = 7\%$ is due to heuristic model, Eq. (18).

and in the opposite limit of weak coherence;

$$\mathcal{E}(M) \approx N_{\mathrm{coh}}[1 - (2\mu)^{-1}], \qquad \mu \gg 1, \tag{16}$$

which indicates that even when the full coherence is lost because of too many elements M, we still have $\mathcal{E} \approx N_{\mathrm{coh}} \gg 1$ enhancement over the case of fully random structure. This result could be readily understood from these qualitative considerations. Let us assume that there is a "coherent block" of elements, which has N_{coh} elements in it, with all of them being ideally equally spaced, so that the gain of that fully coherent block is $G_{\mathrm{bl}} = N_{\mathrm{coh}}^2$, and there are $N_{\mathrm{bl}} = M/N_{\mathrm{coh}}$ of these blocks. Suppose now that these blocks are fully incoherent with each other, so the total gain of the system of these blocks is

$$G_M = N_{bl}G_{bl} = MN_{\mathrm{coh}}, \qquad \mathcal{E}(M) \approx N_{\mathrm{coh}}, \tag{17}$$

which explains Eq. (16) qualitatively and gives a simple picture of the transition from fully randomized to fully coherent situations. Equation (14) shows that when $\mu = 1$ or $M = N_{\mathrm{coh}}$, the system exhibits only ~50% loss of coherency compared with the ideal case [Eq. (1)], thus still providing for the orders-of-magnitude enhancement over the fully randomized case [Eq. (2)].

Amazingly, both Eq. (13) and Eq. (14) can be approximated within less than 5% by a much simpler heuristic formula, which is intuitively transparent and could be useful for practical applications in the entire range of parameters M and N_{coh}:

$$\mathcal{E}_H(M) \approx \frac{MN_{\mathrm{coh}}}{M + N_{\mathrm{coh}} - 1} = \frac{M}{(M-1)r + 1}. \tag{18}$$

The behavior $\mathcal{E}_H(M)$ for $\sigma_0 = 7\%$ (and thus $N_{\mathrm{coh}} \sim 20$) is depicted as curve H in Fig. 1; one can clearly see that it deviates very little from the analytical result for Gaussian distribution.

5. NON-GAUSSIAN STATISTICS AND MONTE-CARLO SIMULATIONS

While analytical results Eq. (13) or Eq. (14) are true, strictly speaking, for the normal (i.e., Gaussian) distribution, they are expected to be true also for any other distribution provided the number $|n - k|$ in Eq. (9) is sufficiently large. Indeed, owing to the central limit theorem, the amount $X_n - X_k = \Sigma_{j=k}^{n} x_j \equiv Y_{nk}$, which is the sum of many uncorrelated random variables x_j having the identical probability distribution, is asymptotically normal, i.e., it has a normal distribution for sufficiently large $|n - k|$ regardless of the distribution of the variables x_j. This condition is automatically satisfied in the case $N_{\mathrm{coh}} = (\pi\sigma_0)^{-2} \gg 1$ or $(\pi\sigma_0)^2 \ll 1$, which is the case for most situations of practical interest. The question then is whether non-Gaussian distributions, which are most likely to happen, would produce significantly different (from Gaussian) results in the case of large standard deviations, $\sigma_0 \sim \pi^{-1}$ or even $\sigma_0 > \pi^{-1}$.

For that purpose, to make sure that our analytic formulas for normal distribution have great precision for any realistic model of the probability distribution of the phase/length of each element in the structure, we run Monte Carlo simulations for a few significantly different non-Gaussian distributions. Note again that, for all the models considered in this section, we made no assumptions as to the behavior of $\langle x_n^2 \rangle$, G_M, $P_{nk}(y)$, and $\langle \cos(2\pi Y_{nk}) \rangle$, and thus no formulas are that applicable, strictly speaking, to the normal distribution [e.g., the second part of Eq. (4) and Eqs. (9)–(11)] were used. Naturally, no analytical results obtained in Sections 2–4 and related to the Gaussian distribution were used here. In each of the simulations we directly evaluated the sum [Eq. (7)] with $\theta = 0$ for any given M and then averaged this summation over the ensemble, using 10^4 or more runs with a random seed for each one of them. Within each of these simulations the phase x_n of each element in the summation was random.

For our tests we have chosen four substantially different probability distributions $P(x)$ for the phase x_n, with $\langle x \rangle = 0$ and $\langle x^2 \rangle = \sigma_0^2$. For the Monte Carlo technique to work, the distribution $P(x) > 0$ should have spatial boundaries

$$P(x) > 0 \begin{cases} \text{for } |x| < \delta^{-1} \\ 0 \text{ otherwise} \end{cases}, \tag{19}$$

where $\delta = \sigma_0 O(1)$. The nonzero parts of the distributions used by us are

(i) rectangular, discontinued distribution:

$$P(x) = \text{const} = 1/2\delta, \qquad \text{with } \delta = \sigma_0\sqrt{3}, \tag{20}$$

(ii) quasi-bell-shaped continued distribution with discontinued derivative at the edges:

$$P(x) = (\pi/4\delta)\cos(\pi x/2\delta), \qquad \text{with } \delta = \sigma_0/(1 - 8/\pi^2)^{1/2} \tag{21}$$

and two "smooth" bell-shaped distributions to closely emulate Gaussian distribution within finite interval $|x| \leqslant \delta$:

(iii) the simplest "$\cos^2$"-distribution:

$$P(x) = \delta^{-1}\cos^2(\pi x/2\delta), \qquad \text{with } \delta = \sigma_0/(1/3 - 2/\pi^2)^{1/2} \tag{22}$$

(iv) and "polynomial" distribution:

$$P(x) = \frac{15}{8\delta}\left(1 - \frac{|x|}{\delta}\right)^2\left[1 - \frac{2}{5}\left(1 - \frac{|x|}{\delta}\right)^3\right], \qquad \text{with } \delta = 4\sigma_0\left(\frac{7}{13}\right)^{1/2}. \tag{23}$$

All of these probability distributions are depicted in Fig. 2, where the dimensionless distributions, $P(x)\sigma_0$, are shown versus the normalized random deviation x/σ_0.

Both distributions (iii) and (iv) are smooth functions in the interval $|x| \leqslant \delta$ [i.e., $P(x)$ and dP/dx are continuous], and zero out, same as their derivatives, at both ends of that interval. Although Eq. (22) is perhaps one of the simplest in this category, Eq. (23) has the advantage of having the equation $r_{\mathrm{rnd}} = W(x)$ analytically solvable for x [same as in Eqs. (20) and (21)], where $0 \leqslant r_{\mathrm{rnd}} \leqslant 1$ is a random number generated by computer for each individual element, and

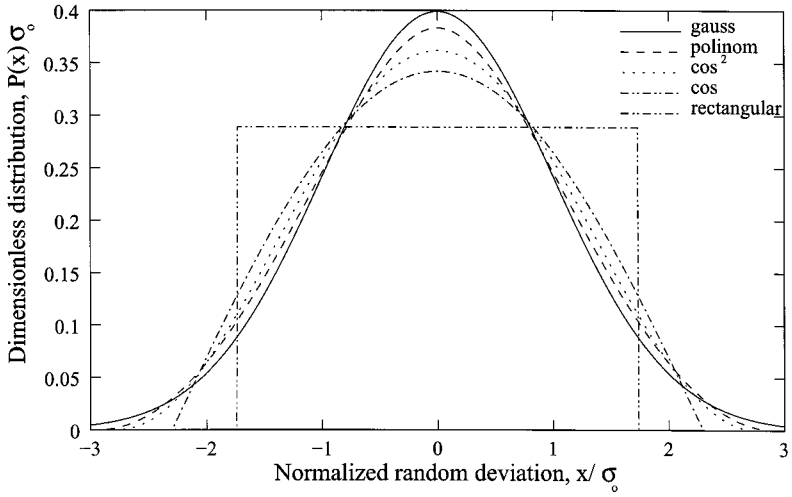

Fig. 2. Various probability distribution models used for calculation in Fig. 1. The solid curve corresponds to a normal (Gaussian) distribution, Eq. (10), the "polinom" corresponds to the model described by Eq. (23), the "$\cos^2$" corresponds to Eq. (22), the "cos" corresponds to Eq. (21), and "rectangular" corresponds to Eq. (20).

$$W(x) = \int_{-\delta}^{x\leqslant\delta} P(\xi)d\xi \qquad r_{\mathrm{rnd}} = \int_{-\delta}^{x\leqslant\delta} P(\xi)\mathrm{d}\xi \quad \text{for } x,$$

is the integral probability; this quality is greatly instrumental in speeding up Monte Carlo simulations. In all of these simulations, we found consistent agreement with Eq. (14), with a precision better then within 5% (most often much better than that) and with the tolerances as large as $\sigma_0 \sim 25\%$ of the individual spacing.

Note that the strong deviations of $\mathcal{E}_M$ for statistical models with non-Gaussian distribution of individual elements from the results for purely Gaussian individual distributions could be expected only near $\sigma_0 \sim 1/\pi$, where they do not make any difference anyway, since for all the practical purposes, the system is almost fully incoherent, i.e., in that limit $\mathcal{E}_M = 1$. In the case $r \ll 1$ (see Eq. (12)), in order for $|n - k|(\pi\sigma_0)^2$ in Eq. (11) to be comparable with 1, one needs $|n - k| \gg 1$, so the assumption that the sum of x_n has a Gaussian distribution, regardless of the individual distributions for the elements, is valid.

Figure 1 depicts a few typical runs for various probability distributions, showing the coherency enhancement $\mathcal{E} = G_M/M$ versus the number of elements M in the structure for various standard deviations σ_0. The upper straight curve $\mathcal{E} = M$ here corresponds to the fully coherent structure ($\sigma_0 = 0$), whereas the constant $\mathcal{E} = 1$ corresponds to the fully randomized structure ($\sigma_0 = \infty$). The rest of the curves correspond to $\sigma_0 = 1\%$, 7%, 15%, and 23% from top to bottom, respectively. Each group of curves corresponding to each specific σ_0 consists of five curves: a solid line is due to the exact analytical result [Eq. (13)] for a strictly Gaussian model of statistical distribution of the spacing, and the rest of them are due to the four models [Eqs. (20)–(23)] obtained by Monte Carlo simulations. All of the models produced the results that deviate very little from Eq. (13); the best coincidences occur for the polynomial model [Eq. (23)]. One can clearly see that the results are very close to each other for all the σ_0 terms we tried. When using the Monte Carlo simulation, after generating the random number r_{rnd} for each element, we found the exact random variable x by analytically solving the equation

and after running the calculations for each structure, made 10^4 statistically independent runs for the ensemble averaging for each point on the curve.

For $\sigma_0 = 1\%$, 7%, 15%, and 23% the coherency ranges are $N_{\mathrm{coh}} \sim 1000$, ~20, ~4, and ~2, respectively. This is a huge coherency span, and our theory held well over all of it. Only at $\sigma_0 = 23\%$ ($N_{\mathrm{coh}} \approx 2$) did the results for various statistical models show some differences. The worst was a rectangular distribution, Eq. (20), with the maximum deviation from the Gaussian case being ~23%; next to the worst was a cosine distribution, Eq. (21), with a maximum deviation of ~15%. Then there was a square-cosine distribution, Eq. (22), with a maximum deviation of ~11%, and finally, the best was a polynomial distribution, Eq. (23), with a maximum deviation of ~8%. However, this case, with $N_{\mathrm{coh}} \approx 2$, corresponds to only near-neighbor coherency, i.e., when the coherency is almost lost, so the differences between models at this point is moot. For the lower σ_0 terms, the results followed the same pattern as far as "the worst" and "the best," but the maximum deviations from the Gaussian distribution were much smaller: ~11%, ~8%, ~6%, and ~5%, for $\sigma_0 = 15\%$, ~4%, ~3.5%, ~3.2%, and ~3%, respectively, for $\sigma_0 = 7\%$; and ~0.3% for all of the models for $\sigma_0 = 1\%$. It is worth noting that as the σ_0 terms become large, $\sigma_0^2 \gg 1$; the results for all of the statistical models coincide with that of the Gaussian model, albeit the trivial reason for that is that the coherent enhancement in this, Archimedes' limit simply disappears, $\mathcal{E} = 1$ and $G = G_{\mathrm{rand}} = M$.

Finally, we have also considered two analytical models of $P(x)$ that would allow for infinite deviation of the phase $2\pi x_n$ in Eq. (3) within Monte Carlo simulations, in contrast to the limited deviations for x, as in Eq. (19), and in all four non-Gaussian models [Eqs. (20)–(23)]. The Monte Carlo simulations with them are possible owing to the fact that, similarly to Eqs. (20), (21), and (23), these two models allow for the analytical solution for x of the equation

$$r_{\mathrm{rnd}} = W(x) \equiv \int_{-\infty}^{x} P(\xi)\mathrm{d}\xi \tag{24}$$

for any given random number $0 \leqslant r_{\mathrm{rnd}} \leqslant 1$. These models are

(v) An inverse square hypebolic sine distribution:

$$P(x) = \frac{1/(2\delta)}{\cosh^2(x/\delta)}, \qquad W(x) = \frac{1}{2} + \frac{\tanh(x/\delta)}{2}, \tag{25}$$

with

$$\frac{\delta}{\sigma_0} = \frac{1}{\sqrt{I_{\mathrm{ch}}}} \approx 1.102658,$$

where

$$I_{\mathrm{ch}} \equiv \int_0^{\infty} \frac{\xi^2 \mathrm{d}\xi}{\cosh^2(\xi)} \approx 0.822467, \tag{26}$$

(vi) and a quasi-Gaussian distribution:

$$P(x) = \frac{1}{2\delta}\left(1 + \frac{|x|}{\delta}\right)\exp\left[-\frac{(1 + |x|/\delta)^2 - 1}{2}\right],$$

$$W(x) = \frac{1}{2} + \frac{\mathrm{sign}(x)}{2} \times \left\{1 - \exp\left[-\frac{(1 + |x|/\delta)^2 - 1}{2}\right]\right\}, \tag{27}$$

where $\mathrm{sign}(x) = x/|x|$ if $|x| > 0$, and $\mathrm{sign}(x) = 0$ otherwise, with

$$\frac{\delta}{\sigma_0} = \frac{1}{\sqrt{I_{qG}}} \approx 1.2050459,$$

where

$$I_{qG} \equiv \int_1^{\infty} \frac{\xi(\xi - 1)^2 \mathrm{d}\xi}{\exp[-(\xi^2 - 1)/2]} \approx 0.6886409. \tag{28}$$

The results of the Monte Carlo simulations for both of these models were very consistent with those for the Gaussian distribution and of the same order of magnitude as the "best" of the the models [Eqs. (20)–(23)]. The main new feature of the models [Eqs. (25) and (27)] was that while the models (20)–(23) showed a coherency slightly lower than that of the Gaussian distribution, the models [Eqs. (25) and (27)] were slightly higher than that. The major parameter indicating how the coherency due to a certain model will differ from that of the Gaussian distribution is whether the peak probability $P(x = 0) = A_m/\sigma_0$ for that model is closer to (and at that higher or lower than) that of the Gaussian distribution, for which $A_m = 1/\sqrt{2\pi}$; this can easily be verified if all the models [Eqs. (20)–(23), (25), and (27)] discussed here are checked.

Our conclusion is that for all practical purposes, there is no need for concern of the specific probability distribution of the random phase and spacing, etc. of a periodical structure; the results for all of the (even drastically) different distributions of practical interest are very close to those for the Gaussian distribution. The only statistical parameter needed for practical estimates and evaluation of the coherency quality of these structures is the standard deviation σ_0 which immediately determines a characteristic scale of the coherent size, of coherency range, of the structure, $N_{\mathrm{coh}} = (\pi\sigma_0)^{-2}$, Eq. (12). Furthermore, the coherent enhancement for all of these distributions including the Gaussian, are well approximated by astonishingly simple heuristic formula [Eq. (18)].

6. ANGULAR AND/OR TEMPORAL DISTRIBUTION OF COHERENCY-SATURATED ARRAY

For applications like spectroscopy, radar and antenna technologies, and generation of short pulses, etc, one needs also to know how coherence saturation affects or broadens the spatial lobe (diagram) of radiation. For this, one has to consider a full-blown case with $\theta \neq 0$ in Eq. (9). By introducing the notation

$$d = \pi\theta, \tag{29}$$

using the same line of calculations as in Eq. (13), and replacing the resulting sums by integrals, since we are interested only in the case $r \ll 1$, similarly to Eq. (14) we arrive at the relationship

$$\mathcal{E}_M(r, d) \equiv \frac{G_M}{M} = \frac{r}{d^2 + r^2} - \frac{\exp(-rM)}{M(d^2 + r^2)^2} \times \{(r^2 - d^2)[\sinh(rM) - \exp(-rM)\sin^2(dM)] + rd\exp(-rM)\sin(2dM)\}. \tag{30}$$

For $d = 0$, Eq. (30) reduces to Eq. (14), as expected; for $r = 0$, we also have, as expected;

$$G_M = \sin^2(dM)/d^2, \tag{31}$$

so a half-width $d_{1/2}$ of the prime lobe at the level $G_M = M^2/2$ is

$$d_{1/2} \approx \sqrt{2}/M. \tag{32}$$

We expect it to increase once $r \neq 0$. Figure 3 depicts G_M versus the detuning θ for various standard deviations $\sigma_0 = 0$, 0.5%, 1%, and 1.5% in the case of $M = 1000$.

In the limiting case of highly saturated coherency, $M \gg N_{\mathrm{coh}}$, or $\mu \gg 1$, the oscillating and some other terms in Eq. (30) become insignificant, and it can be written as

$$\mathcal{E}_M \approx \frac{r(1 + \Delta)}{d^2 + r^2}, \tag{33a}$$

where

$$\Delta = \mu^{-1}O(1) = \frac{d^2 - r^2}{\mu(d^2 + r^2)}. \tag{33b}$$

In the limit $\mu \to \infty$, we have

$$\mathcal{E}_M \approx r/(d^2 + r^2), \qquad d_{1/2} \approx r = N_{\mathrm{coh}}^{-1} = (\pi\sigma_0)^2. \tag{34}$$

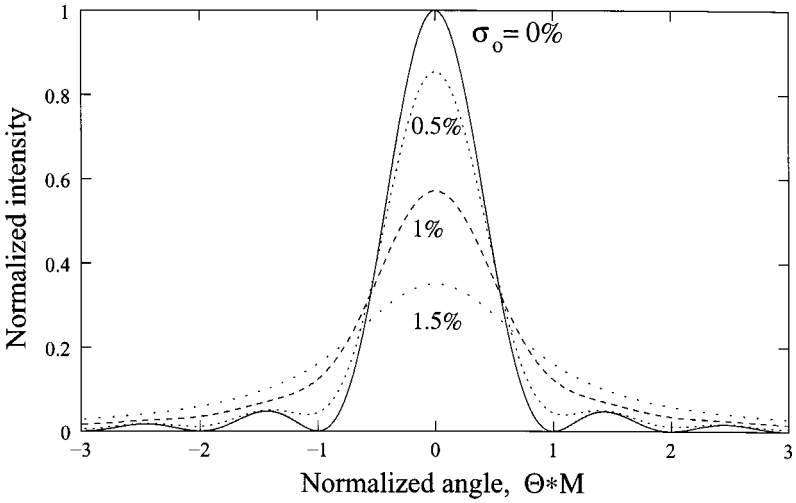

Fig. 3. The coherency gain G_M versus the detuning/angle θ for various standard deviations σ_0 in the case $M = 1000$. The solid curve corresponds to the ideally coherent grating $\sigma_0 = 0$.

Using the notion of coherency radius R_{coh}, which in our case can be defined as $R_{\mathrm{coh}} = N_{\mathrm{coh}} l_0$, often used in the theory of randomized nonlayered structures, we can see that if $l_0 = \lambda/2 = \pi/k$, Eq. (34) coincides with the relation $\theta_{1/2} \approx 1/kR_{\mathrm{coh}}$, well known in the random field and antenna theories.[35]

In the entire domain of r and M, a good approximation for the half-width of the prime lobe with $r \neq 0$, useful for practical estimates, is

$$d_{1/2} = \pi\theta_{1/2} \approx \frac{1}{M}\left[1 + \exp\left(-\frac{2M}{N_{\mathrm{coh}}}\right)\right]^{1/2} + \frac{1}{N_{\mathrm{coh}}} = \frac{[1 + \exp(-2Mr)]^{1/2}}{M} + r. \tag{35}$$

7. COHERENCY SATURATION OF TRANSITION RADIATION IN A SOLID-STATE LAYERED STRUCTURE

Let us consider a specific application of the general result, Eq. (14), to the so-called resonant transition radiation (RTR) emitted when the electrons traverse a spatially periodic stack of layers with alternating dielectric constants. There is a great deal of work on the subject (see, e.g., Refs. 36 and 37) that is based on the use of a stock of metal foils in vacuum or air, and very high energies E_e of electron beams (typically a few giga-electron-volts). For the use of relatively low energies E_e (from sub-mega-electron-volts to a few mega-electron-volts), which can be obtained on widely available industrial, medical, and university accelerators and greatly increase the efficiency of the RTR emission by use of a huge contrast of refractive indexes near the atomic absorption edges of constituting materials, it was proposed[38–41] to use multilayer solid-state structures with nanospacing between layers and with the material chosen to have atomic edges in the vicinity of specifically designated energies.

For medical applications of RTR, mega-electron-volt electron beams are required, and the expected radiation is in the hard-x-ray domain (typically, a few tens of kilo-electron-volts), the thickness of each element, or "period" (a combination of two layers, one the so-called spacer, and another, the so-called radiator, both of them of the same thickness), can vary from ~100 Å to a few hundreds of angstroms. Let us estimate the expected enhancement for the specific example of Mo near its main K-shell transition (atomic absorption edge) at 20 KeV, which corresponds to the wavelength of $\lambda \sim 0.62$ Å. Using the theory in Ref. 41, we have the phase difference ϕ between the adjacent periods of the multilayer structure:

$$\phi \approx \pi(\gamma^{-2} + \theta^2)(l_0/\lambda), \tag{36}$$

with $\phi = 2\pi$ yielding the exact resonant condition. Here θ is the angle of transition radiation at the wavelength λ and $\gamma = E/mc^2$ is the relativistic factor of electrons. It was shown in Ref. 31 that the optimum condition corresponds also to $\theta = 1/\gamma$, so that Eq. (36) with $\phi = 2\pi$ produces a simplified formula for the optimal thickness of one individual period of the structure:

$$l_0 = \lambda \times \gamma^2, \qquad S = 1/\gamma^2, \tag{37}$$

see Eq. (3). For the energy of electron beam ~10 MeV or $\gamma \approx 20$, we have $l_0 \approx \lambda \times 400 \approx 248$ Å. Assuming $\sigma_l \sim 2.48$ Å tolerance in the thickness l_0 of each individual period, one has the standard relative deviation $\sigma_0 \sim 1\%$ and the coherency range $N_{\mathrm{coh}} \sim 10^3$, so with the total number of periods $M \sim 10^2$, one has a gain G only 7% below the fully coherent $G = 10^4$; see Eq. (15). With $M \sim 10^3$, one has ~50% of the fully-coherent $G = 10^6$, which is a huge number. With the energy 5 MeV, the period thickness is $l_0 \sim 62$ Å, and for $\sigma_l = 1$ Å one has $\sigma_0 = 1.6\%$ and $N_{\mathrm{coh}} \sim 400$, so for $M \sim 100$ one has $G \sim 0.8 \times 10^4$, [Eq. (14)], which is 80% of the fully coherent $G = 10^4$ and thus is a great enhancement over the fully incoherent $G = 10^2$. With $M = 400$ for the same energy, we have $G \sim 0.8 \times 10^5$, which by more than 3 orders of magnitude exceeds $G_{\mathrm{rand}} = 400$. The total standard deviation of the structure with the number of elements M and total thickness $L = Ml_0$ is

$$\sigma_L = \sqrt{M}\sigma_l, \qquad \text{or} \quad \sigma_L/L = \sigma_0/\sqrt{M}. \tag{38}$$

In an above example with $l_0 = 248\,\text{Å}$, $\sigma_l \sim 2.48\,\text{Å}$, and $M = 100$, one has $\sigma_L \sim 24.8\,\text{Å}$ over $L = 2.48\ \mu\text{m}$. Note here that the quantity σ_L is not a tolerance requirement; it comes out simply as a statistical consequence of the only tolerance, that for a single element or period, σ_l.

Note also that at the energies of the electron beam used here, the frequencies of x-ray radiation, and the presumed number of periods, the total thickness of the structure ($\sim$1–2 μm) is much smaller than both the photoabsorption length ($\sim$12 μm for Mb) and the electron scattering length (more than 1 mm),[40,41] so both of these processes were neglected in our estimates here.

8. CONCLUSION

In conclusion, we demonstrated that within a very generic statistical model of randomized quasi-periodic radiative/reflecting/transmitting arrays and structures, their coherency can be described by very simple formulas that show its saturation as the number of radiative/reflecting elements in the structure exceeds a certain coherency range that is inversely proportional to the square of the standard deviation of the spacing from the design length. We found that regardless of the specific model of the statistical distribution of the random phase deviation in the structure, the resulting coherency is described with great precision by normal (Gaussian) distribution with the same standard deviation. In most of the cases of practical interest, the coherency range is sufficiently high to provide for a very robust coherent behavior and allows one to use up to a few hundreds of layers even in a hard x-ray domain without a significant loss of radiation coherency.

We greatly appreciate fruitful discussions with E. Wolf, V. I. Tatarsky, P. L. Shkolnikov, and Y. A. Kravtsov. This work is supported by AFOSR.

A.E. Kaplan's e-mail address is sasha @striky.ece.jhu.edu.

REFERENCES

1. Ya. S. Shifrin, *Statistical Antenna Theory* (Golem, Boulder, Co., 1971).
2. M. Kominami and K. Rokushima, "Analysis of an antenna composed of arbitrarily located slots and wires," IEEE Trans. Antennas Propag. **32**, 154–158 (1984).
3. W. J. Hendricks, "The totally random versus the bin approach for random arrays," IEEE Trans. Antennas Propag. **39**, 1757–1762 (1991).
4. T. Lyman, "False spectra from the Rowland concave grating," Phys. Rev. **12**, 1 (1901).
5. R. Wood, "Anomalous diffraction gratings," Astrophys. J. **48**, 928 (1935).
6. J. Rossi and D. Maystre, "Light scattering by diffraction gratings, false gratings and random rough surfaces: numerical comparison," J. Opt. Soc. Am. A **17**, 165–173 (1986).
7. D. Photiadis, "The effect of irregularity on the scattering of acoustic waves from a ribbed plate," J. Acoust. Soc. Am. **91**, 1897–1903 (1992).
8. B. Cray, "Acoustic radiation from periodic and sectionally aperiodic rib-stiffened plates," J. Acoust. Soc. Am. **95**, 256–264 (1994).
9. D. Hughes, C. Gaumond, L. Dragonette, and B. Houston, "Synthesized wave-packet basis for monostatic scattering-from a randomly ribbed, finite cylindrical-shell," J. Acoust. Soc. Am. **97**, 1399–1408 (1995).
10. J. Albert, S. Theriault, F. Bilodeau, D. C. Johnson, K. O. Hill, P. Sixt, and M. J. Rooks, "Minimization of phase errors in long fiber Bragg grating phase masks made using electron beam lithography," IEEE Photonics Technol. Lett. **8**, 1334–1336 (1996).
11. E. Spiller, "Coherence effects from visible light to X-rays," Nucl. Instrum. Methods **347**, 161–169 (1994).
12. E. Spiller, D. Stearns, and M. Krumrey, "Multilayer X-ray mirrors—interfacial roughness, scattering, and image quality," J. Appl. Phys. **74**, 107–118 (1993).
13. T. W. Barbee, "Multilayer optics for the soft-X-ray and extreme ultra-violet," Phys. Scr. **31**, 147–153 (1990).
14. E. Esarey, C. Tang, and W. Marable, "The effects of field errors on low-gain free-electron lasers," IEEE J. Quantum Electron. **27**, 2682–2692 (1991).
15. M. Takao, S. Hashimoto, S. Sasaki, and Y. Miyahara, "Analytical formulation of a quasi-periodic ondulator," in *Proceedings of the Particle Accelerator Conference* (Institute of Electrical and Electronics Engineers, Piscataway, N.J., 1995), Vol. 3, pp. 1438–1440.
16. P. Emma, "Phase slip in an ondulator with pole and BPM errors," in *Proceedings of the Particle Accelerator Conference*, (Institute of Electrical and Electronics Engineers, Piscataway, N.J., 2001), Vol. 4, pp. 2742–2744.
17. G. Garibian, L. Gevorgian, and C. Yang, "Calculation of X-ray transition radiation generated in regular-layered and irregular-layered media," Nucl. Instrum. Methods **125**, 133–137 (1975).
18. C. Fabjan, "Transition radiation spectra from randomly spaced interfaces," Nucl. Instrum. Methods **146**, 343–346 (1977).
19. Z. Gevorkian, C. Chen, and C. Hu, "New mechanism of x-ray radiation from a relativistic charged particle in a dielectric random medium," Phys. Rev. Lett. **86**, 3324–3327 (2001).
20. K. Platonov and G. Fleishman, "Transition radiation in media with random inhomogeneities," Phys. Usp. **45**, 235–291 (2002).
21. Y. Yamakoshi, K. Muto, and Z. Yoshida, "Numerical analysis of quasi-periodic perturbations for the Alfvén-wave," Phys. Rev. E **50**, 1437–1444 (1994).
22. R. Grisenti, W. Schöllkopf, J. Toennies, J. R. Manson, T. A. Savas, and H. I. Smith, "He-atom diffraction from nanostructure transmission gratings: the role of imperfections," Phys. Rev. A **61**, 33608–33612 (2000).
23. E. Yablonovitch, "Inhibited spontaneous emission in solid-state physics and electronics," Phys. Rev. Lett. **58**, 2059–2062 (1987).
24. E. Yablonovitch and T. G. Gmitter, "Photonics band-structure," Phys. Rev. Lett. **63**, 1950–1953 (1989).
25. S. H. Fan, P. R. Villeneuve, and J. D. Joannopoulos, "Theoretical investigation of fabrication-related disorder on the properties of photonic crystals," J. Appl. Phys. **78**, 1415–1418 (1995).
26. A. Siegman, *Lasers* (University Science, 1986).
27. P. M. Paul, E. S. Toma, P. Breger, G. Mullot, F. Auge', Ph. Balcou, H. G. Muller, and P. Agostini, "Observation of a train of attosecond pulses from high harmonic generation," Science **292**, 1689–1692 (2001).
28. M. Hentschel, R. Kienberger, C. Spielmann, G. A. Reider, N. Milosevic, T. Brabec, P. Corkum, U. Heinzmann, M. Drescher, and F. Krausz, "Attosecond metrology," Nature (London) **414**, 509–513 (2001).
29. A. E. Kaplan, "Subfemtosecond pulses in mode-locked 2π solitons of the cascade stimulated Raman scattering," Phys. Rev. Lett. **73**, 1243–1246 (1994).
30. A. E. Kaplan and P. L. Shkolnikov, "Subfemtosecond pulses in the multi-cascade stimulated Raman Scattering," J. Opt. Soc. Am. B **13**, 347–354 (1996).
31. S. E. Harris and A. V. Sokolov, "Subfemtosecond pulse generation by molecular modulation," Phys. Rev. Lett. **81**, 2894–2897 (1998).
32. M. Sebastian and P. Krishna, *Random, Non-Random and Periodic Faulting in Crystals* (Gordon and Breach, New York, 1994).

33. J. Sasaki, L. Cardoso, C. Campos, K. Roberts, G. Clark, E. Pantos, and M. Sacilotti, "Using synchrotron radiation x-ray multiple diffraction to examine the lattice coherency of semiconductor surfaces and epitaxial layers," J. Appl. Phys. **79**, 34923498 (1996).
34. T. Valla, P. Johnson, Z. Yusof, B. Wells, Q. Li, S. Loureiro, R. Cava, M. Mikami, Y. Mori, M. Yoshimura, and T. Sasaki, "Coherence–incoherence and dimensional crossover in layered strongly correlated metals," Nature **417**, 627–630 (2002).
35. S. M. Rytov, Y. A. Kravtsov, and V. I. Tatarskii, *Principles of Statistical Radiophysics*, "Elements of random fields" (Springer-Verlag, Berlin, 1989), Vol. 3.
36. M. L. Ter-Mikaelian, *High Energy Electromagnetic Processes in Condensed Media* (Wiley Interscience, New York, 1972).
37. M. L. Ter-Mikhaelyan, "Electromagnetic radiative processes in periodic media at high energies," Phys. Usp. **44**, 571–596 (2001).
38. A. E. Kaplan and S. Datta, "Extreme-ultraviolet and x-ray emission and amplification by non-relativistic beams traversing a superlattice," Appl. Phys. Lett. **44**, 661–663 (1984).
39. S. Datta and A. E. Kaplan, "Quantum theory of spontaneous and stimulated resonant transition radiation," Phys. Rev. A **31**, 790–796 (1985).
40. C. T. Law and A. E. Kaplan, "X-ray transition radiation in a solid-state superlattice: photon-absorption, electron scattering, and radiation optimization," Opt. Lett. **12**, 900–902 (1987).
41. A. E. Kaplan, C. T. Law, and P. L. Shkolnikov, "X-ray narrow-line transition radiation source based on low-energy electron beams traversing a multilayer nanostructure," Phys. Rev. E **52**, 6795–6808 (1995).